This copy is for personal use only. To order printed copies, contact *reprints@rsna.org*

Automated Critical Test Findings Identification and Online Notification System Using Artificial Intelligence in Imaging[1]

Luciano M. Prevedello, MD, MPH
Barbaros S. Erdal, PhD
John L. Ryu, MD
Kevin J. Little, PhD
Mutlu Demirer, PhD, MBA
Songyue Qian, BS
Richard D. White, MD

Purpose: To evaluate the performance of an artificial intelligence (AI) tool using a deep learning algorithm for detecting hemorrhage, mass effect, or hydrocephalus (HMH) at non—contrast material–enhanced head computed tomographic (CT) examinations and to determine algorithm performance for detection of suspected acute infarct (SAI).

Materials and Methods: This HIPAA-compliant retrospective study was completed after institutional review board approval. A training and validation dataset of noncontrast-enhanced head CT examinations that comprised 100 examinations of HMH, 22 of SAI, and 124 of noncritical findings was obtained resulting in 2583 representative images. Examinations were processed by using a convolutional neural network (deep learning) using two different window and level configurations (brain window and stroke window). AI algorithm performance was tested on a separate dataset containing 50 examinations with HMH findings, 15 with SAI findings, and 35 with noncritical findings.

Results: Final algorithm performance for HMH showed 90% (45 of 50) sensitivity (95% confidence interval [CI]: 78%, 97%) and 85% (68 of 80) specificity (95% CI: 76%, 92%), with area under the receiver operating characteristic curve (AUC) of 0.91 with the brain window. For SAI, the best performance was achieved with the stroke window showing 62% (13 of 21) sensitivity (95% CI: 38%, 82%) and 96% (27 of 28) specificity (95% CI: 82%, 100%), with AUC of 0.81.

Conclusion: AI using deep learning demonstrates promise for detecting critical findings at noncontrast-enhanced head CT. A dedicated algorithm was required to detect SAI. Detection of SAI showed lower sensitivity in comparison to detection of HMH, but showed reasonable performance. Findings support further investigation of the algorithm in a controlled and prospective clinical setting to determine whether it can independently screen noncontrast-enhanced head CT examinations and notify the interpreting radiologist of critical findings.

©RSNA, 2017

Online supplemental material is available for this article.

[1] From the Department of Radiology, The Ohio State University Wexner Medical Center, 395 W 12th Ave, 4th Floor, Room 422, Columbus, OH 43210. From the 2016 RSNA Annual Meeting. Received November 20, 2016; revision requested January 23, 2017; revision received February 27; accepted March 29; final version accepted April 6.
Address correspondence to L.M.P. (e-mail: *Luciano.Prevedello@osumc.edu*).

This work was supported by the Edward J. DeBartolo, Jr Family.

©RSNA, 2017

A major obstacle to communicating critical imaging results in busy radiology practices relates to delay in recognizing which examinations, out of the many needing review, contain urgent findings. In large academic practices, approximately 40% of all inpatient imaging examinations are designated as needing immediate attention during ordering (1), but no automated method currently exists to proactively triage these examinations on the basis of the true urgency of the imaging findings. Many methods have been previously created to classify critical imaging findings at non—contrast material–enhanced head computed tomographic (CT) examinations. However, the complexity of building and implementing these algorithms, along with their narrow clinical focus, may have contributed to their limited availability.

More recently, artificial intelligence (AI) using deep learning techniques, such as convolutional neural networks, has received extensive attention after demonstrations that it could perform at least as well as humans in imaging classification tasks (2–4). In addition, these algorithms can autonomously "learn" how to classify images on the basis of manually classified initial data. In the field of radiology, this has generated concern that AI could eventually replace the interpretive duties of radiologists (5). However, these speculations have been based on algorithm performance outside of the medical domain, and it remains far from fully recognized how these algorithms will perform in radiology (6).

The purpose of this study was to evaluate the performance of a deep learning AI algorithm to detect critical test findings within a range of noncontrast-enhanced head CT examinations, thereby performing an initial assessment of an Automated Critical Test Findings Identification and Online Notification System, or ACTIONS, to assist radiologists in this important responsibility.

Advances in Knowledge

- Artificial intelligence (AI) with deep learning algorithms can be highly accurate (area under the receiver operating characteristic curve [AUC] = 0.91) in detecting critical findings including hemorrhage, mass effect, and hydrocephalus at noncontrast-enhanced head CT.
- While detection of suspected acute infarct was relatively less accurate (AUC = 0.81), despite use of a dedicated deep learning algorithm, the yield matched previously reported performances of both radiologists and computerized algorithms to detect early ischemic signs.

Implication for Patient Care

- By automating and standardizing several imaging classification tasks, AI may become a key component of radiology workflow optimization in facilitating earlier detection and prompt communication of critical findings.

Materials and Methods

This Health Insurance Portability and Accountability Act–compliant retrospective study was conducted with institutional review board approval and with a waiver of informed consent.

AI Algorithm Development

On the basis of the radiology practice at our institution, some of the most important categories for the identification of critical imaging findings at noncontrast-enhanced head CT examination include the following: category 1, acute hemorrhage; category 2, mass effect; category 3, hydrocephalus; category 4, suspected acute infarct; category 5, encephalomalacia; and category 6, other nonurgent abnormality or normal finding. When new or unexpected, categories 1–4 represent critical imaging results requiring immediate direct communication to the responsible clinical service.

Because routine clinical practice experience indicates that the disease entities in categories 1–3 are generally better delineated with brain window settings (window width, 90 HU; window center, 40 HU), while those in categories 4–5 are better distinguished with stroke window settings (window width, 30 HU; window center, 30 HU), we anticipated the need for two AI algorithms with the intent of using them in a serial deployment strategy as depicted in Figure 1a.

Evaluation of our proposed AI algorithms then followed a typical machine learning algorithm development process as described in Appendix E1 (online).

AI Algorithm Training and Validation

A total of 500 consecutive noncontrast-enhanced head CT examinations (performed in January 2015) available from the institution's picture archiving and communication system were initially considered. All examinations performed at a different institution and subsequently imported into the picture archiving and communication system without supportive clinical information (n = 19) were excluded. Motion-degraded, slanted, and postoperative studies were included to represent standard practice.

The remaining 481 noncontrast-enhanced head CT examinations (93% [449 of 481] performed with Siemens

https://doi.org/10.1148/radiol.2017162664

Content code: NR

Radiology 2017; 285:923–931

Abbreviations:
AI = artificial intelligence
AUC = area under the receiver operating characteristic curve
CI = confidence interval

Author contributions:
Guarantors of integrity of entire study, L.M.P., B.S.E.; study concepts/study design or data acquisition or data analysis/interpretation, all authors; manuscript drafting or manuscript revision for important intellectual content, all authors; approval of final version of submitted manuscript, all authors; agrees to ensure any questions related to the work are appropriately resolved, all authors; literature research, L.M.P., B.S.E., J.L.R.; clinical studies, L.M.P., B.S.E., K.J.L., S.Q., R.D.W.; statistical analysis, L.M.P., S.Q., R.D.W.; and manuscript editing, L.M.P., B.S.E., J.L.R., K.J.L., M.D., R.D.W.

Conflicts of interest are listed at the end of this article.

See also the editorial by Kahn in this issue.

Figure 1

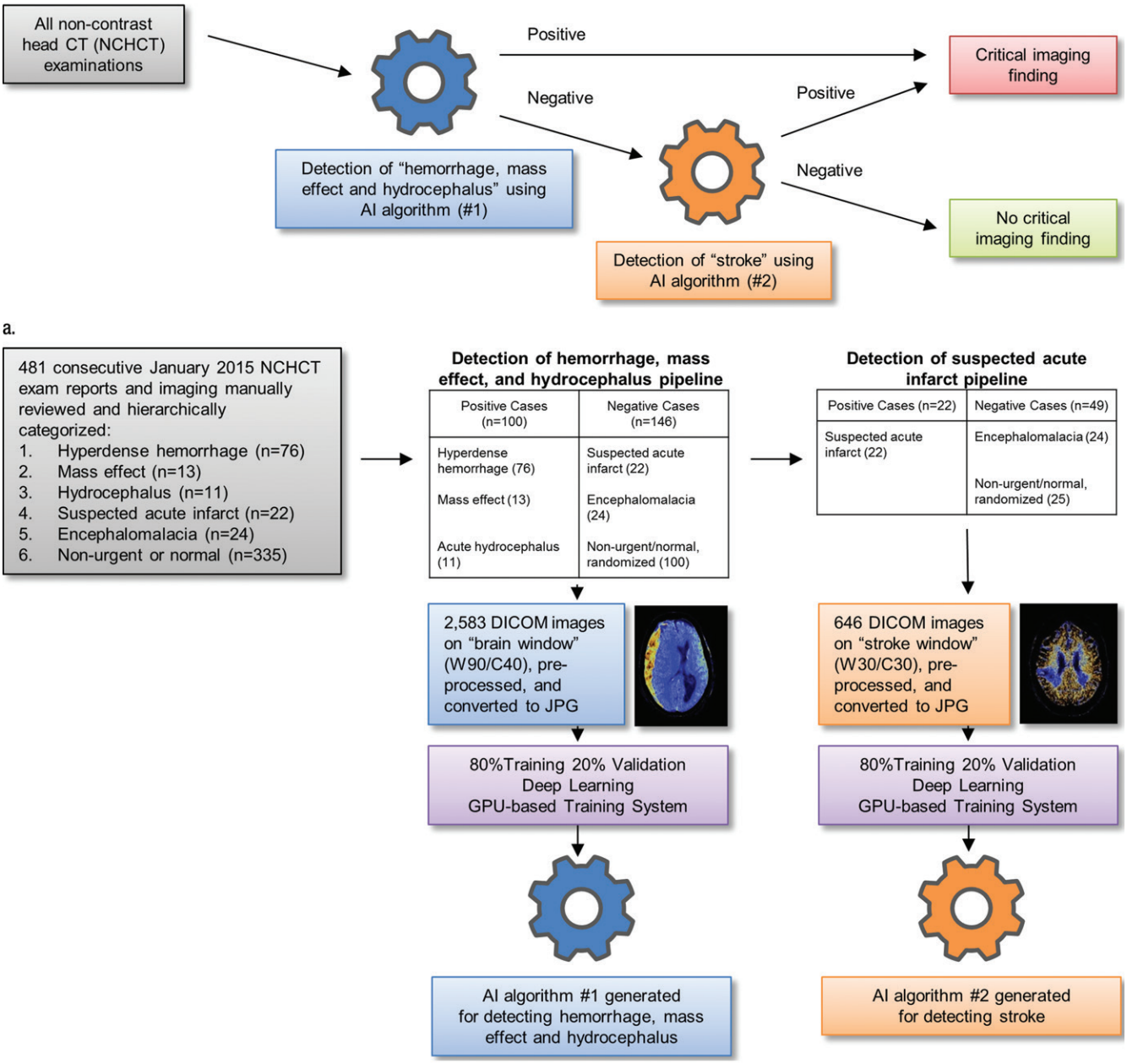

Figure 1: **(a)** Conceptual algorithm deployment strategy. *(Fig 1 continues).*

Somatom systems [Forchheim, Germany]), representing a wide range of neurologic disease entities, were hierarchically arranged into the aforementioned six categories: hyperattenuating hemorrhage ($n = 76$), mass effect ($n = 13$), hydrocephalus ($n = 11$), suspected acute infarct ($n = 22$), encephalomalacia ($n = 24$), and other nonurgent abnormality or normal finding ($n = 335$) as shown in Figure 1b. Studies were assigned to a single category by using a hierarchical distribution (hemorrhage > mass effect > hydrocephalus > suspected acute infarct > nonurgent). This categorization was primarily based on review of the final radiology report (J.L.R., 2nd-year diagnostic radiology resident) by searching for explicit mention of the abnormality in the report. Examinations showing equivocal findings were also reviewed by a board-certified neuroradiologist (L.M.P., with 13 years of postresidency experience) who

Figure 1 (continued)

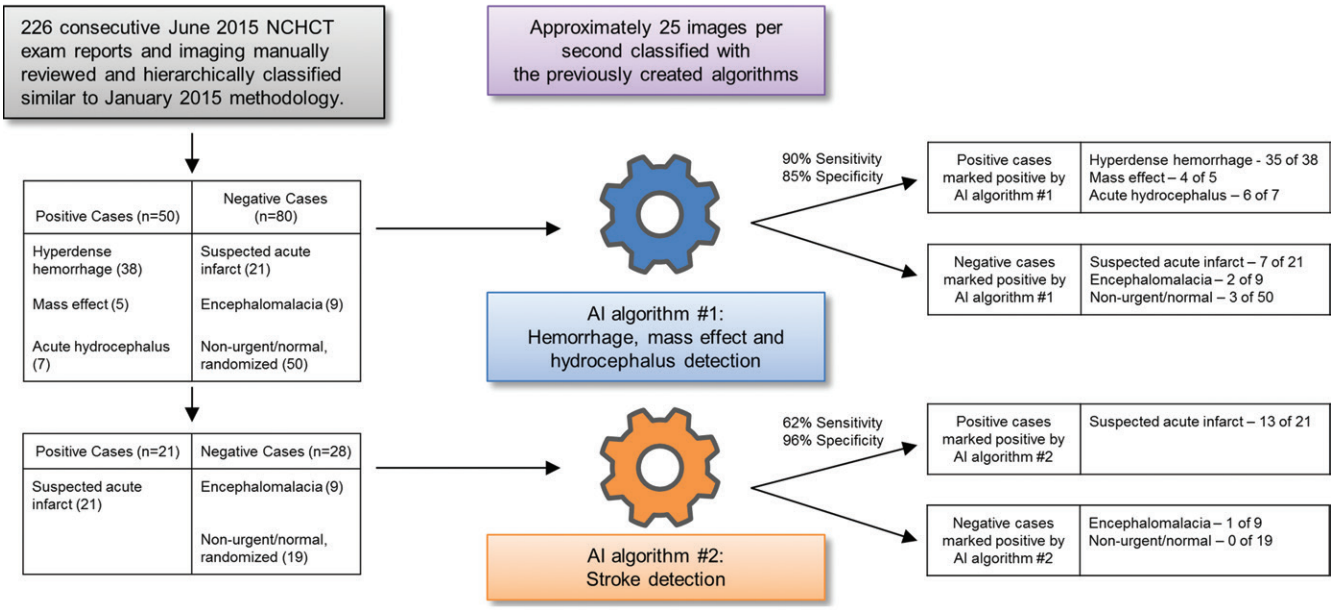

c.

Figure 1 *(continued)*: AI algorithm **(b)** generation and **(c)** evaluation for detecting acute findings at noncontrast-enhanced head CT *(NCHCT)* examinations. *DICOM* = Digital Imaging and Communications in Medicine, *GPU* = graphics processing unit, *JPG* = Joint Photographic Experts Group.

Table 1

Distribution of Patient Age and Sex and Percentage of Critical Imaging Findings Available in Each Dataset

	Age		Sex		Critical Findings	
Algorithm and Dataset	Mean Age (y)*	*P* Value	Percentage of Women†	*P* Value	Percentage of Critical Findings†	*P* Value
Algorithm 1 for hemorrhage, mass effect, or hydrocephalus		.14		.60		.16
Training	60.8 (58.4, 63.3)		43.09 (106/246)		49.6 (122/246)	
Validation	60.3 (57.6, 63.0)		45.5 (91/109)		44 (88/200)	
Test	56.7 (53.3, 60.1)		48.46 (63/160)		54.6 (71/130)	
Algorithm 2 for suspected acute infarct		.83		.17		.11
Training	59.9 (55.7, 64.2)		40.3 (29/72)		30.6 (22/72)	
Validation	57.9 (52.9, 62.9)		43.1 (22/51)		23.5 (12/51)	
Test	58.7 (53.6, 63.8)		57.1 (28/49)		42.9 (21/49)	

* Data in parentheses are 95% CIs.

† Data are percentages, with raw data in parentheses.

assigned the final category on the basis of the images and final report.

To compensate for the skewed distribution favoring noncritical examinations (categories 5–6, $n = 359$) relative to critical examinations (categories 1–4, $n = 122$) and the potential for overtraining of the AI algorithm on the majority class (category 6 in this population) (7), a randomly selected sample of 100 category 6 examinations was collected to help compose a more balanced final training-validation population of critical ($n = 122$) and noncritical ($n = 124$) examinations. Final patient population distribution included categories 1–3 ($n = 100$), category 4 ($n = 22$), and categories 5–6 ($n = 124$). From this 246-examination training-validation population, a total of 2583 representative images were created by using the brain window setting and 646 were created by using the stroke window setting as shown in Figure 1b. These two datasets were further subdivided into a training set (80% of randomly chosen images) and a validation set (remaining 20% of images).

After machine learning training, the two AI algorithms were initially validated for their abilities to correctly

classify examinations by category group (1–3 vs 4–6 with brain window and 4 vs 5–6 with stroke window) in accordance with the previously described strategy.

AI Algorithm Testing

To avoid introduction of selection bias by inclusion of patients who were part of the algorithm training and/or validation cohort, we performed final testing of the algorithms on a separate cohort of noncontrast-enhanced head CT examinations. As shown in Figure 1c, a total of 226 new examinations (performed in June 2015) were consecutively reviewed and similarly classified into the same six categories as used during training and validation. This test dataset included 71 examinations containing critical test findings from categories 1–3 (n = 50) or category 4 (n = 21), as well as 59 noncritical examination findings from category 5 (n = 9) or category 6 (n = 50, randomly selected from unused 146 initial category 6 examinations described earlier). Manual review of the false-positive and false-negative results was performed in the test dataset.

Statistical Analysis

The 95% confidence intervals (CIs) were based on Wilson score intervals. Receiver operating characteristic curves were produced in an open source platform (KNIME, version 3.3.1; KNIME, Zurich, Switzerland). Comparison of the distributions of patient age and sex, along with the percentage of critical imaging findings available in each of the datasets (training, validation, and test), were tested by using analysis of variance for continuous and χ^2 test for categorical variables by using software (JMP Pro, version 12; SAS Institute, Cary, NC).

Results

Table 1 demonstrates no significant difference in the distribution of patient age and sex, along with the percentage of critical imaging findings available in each of the datasets (training, validation, and test sets).

Table 2 shows performance results for the two final algorithms. Final algorithm performance for categories 1–3 showed 90% (45 of 50) sensitivity (95% CI: 78%, 97%) and 85% (68 of 80) specificity (95% CI: 76%, 92%), with AUC of 0.91 with the brain window setting. For category 4, the best performance was obtained with the stroke window setting, showing 62% (13 of 21) sensitivity (95% CI: 38%, 82%) and 96% (27 of 28) specificity (95% CI: 82%, 100%), with AUC of 0.81.

Figure 2 demonstrates the receiver operating characteristic curve illustrating algorithm performance as the predictive probability thresholds change for both algorithms. Figure 3 exemplifies

Table 2

Results of Algorithm Testing

Algorithm and Window Type	Sensitivity (%)	Specificity (%)	AUC
Algorithm 1 for hemorrhage, mass effect, or hydrocephalus (brain window)	90 (45/50) [78%, 97%]	85 (68/80) [76%, 92%]	0.91
Algorithm 2 for suspected acute infarct (stroke window)	62 (13/21) [38%, 82%]	96 (27/28) [82%, 100%]	0.81

Note.—Unless otherwise indicated, date are percentages, with raw data in parentheses and 95% CIs in brackets. AUC = area under the receiver operating characteristic curve.

Figure 2

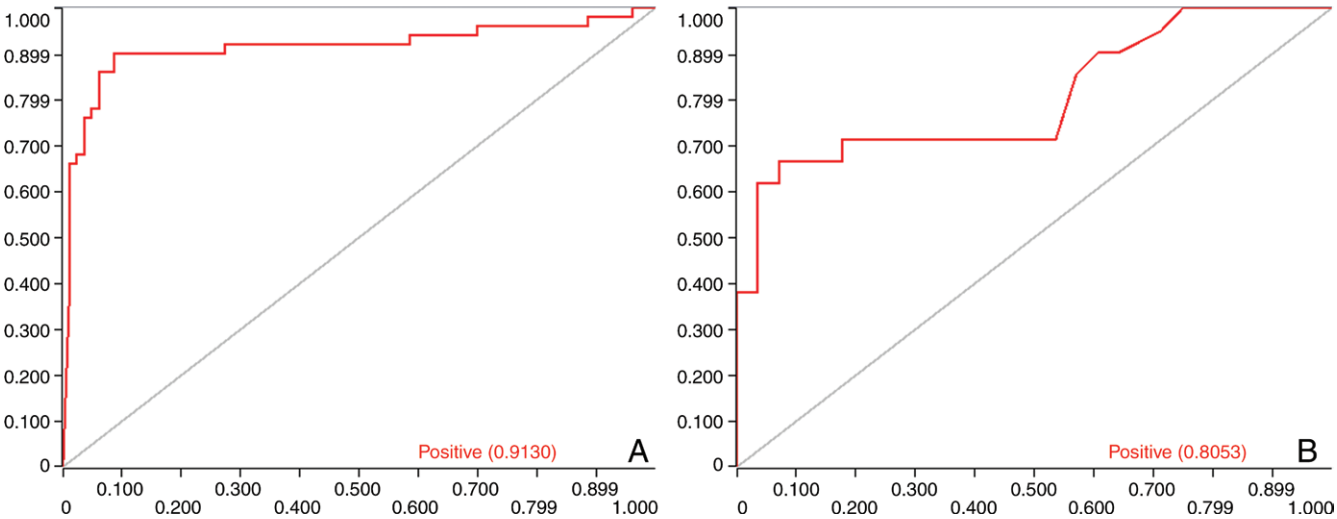

Figure 2: Receiver operating characteristic curve analysis for the two final algorithms. *A,* Detection of hemorrhage, mass effect, and hydrocephalus by algorithm 1. *B,* Detection of suspected acute infarct by algorithm 2. Y-axis represents the true-positive rate (sensitivity), and x-axis represents the false-positive rate (1 − specificity).

Figure 3

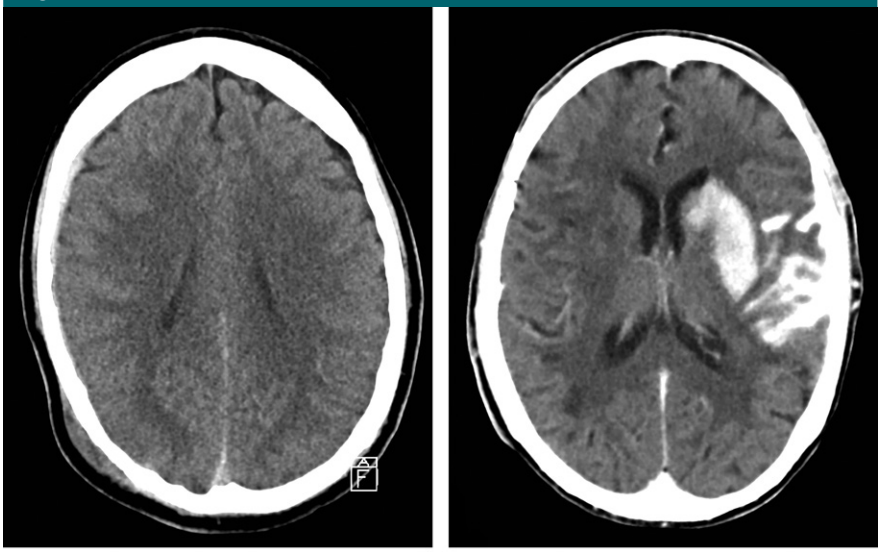

a. b.

Figure 3: **(a, b)** Sample axial CT images from two examinations from the test set with brain window settings (window width, 90 HU; window center, 40 HU). The AI algorithm 1 predicted that **a** (tiny right convexity subdural hematoma) had an 80% chance of containing a critical finding and **b** (hemorrhagic transformation of a left middle cerebral artery infarct with persistent contrast material staining) had a 100% chance of containing a critical finding according to the same algorithm.

Figure 4

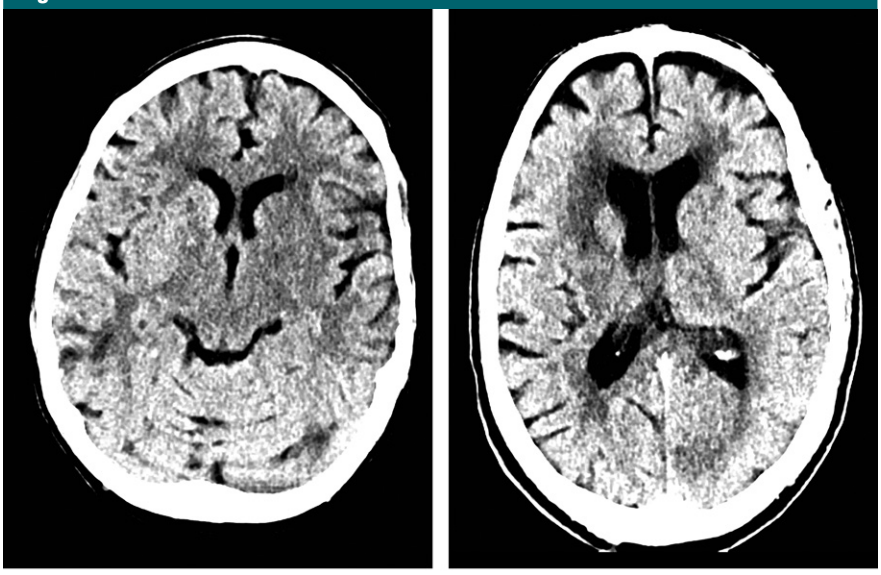

a. b.

Figure 4: **(a, b)** Sample axial CT images from two examinations from the test set manually classified as suspected acute infarct with stroke window settings (window width, 30 HU; window center, 30 HU). The stroke AI algorithm 2 incorrectly predicted that **a** (left middle cerebral artery infarct) had a 1% chance of containing a critical finding and **b** (left posterior cerebral artery infarct) had a 57% chance of containing a critical finding according to the same algorithm.

the predictions obtained with algorithm 1, and Figure 4 shows example results for algorithm 2. A total of five false-negative and five false-positive examination results are presented on Figure 5a–5e and Figure 6a–6e, respectively.

Discussion

In this study, our AI method demonstrated a high performance level in the detection of hemorrhage, mass effect, and hydrocephalus, with lower, but reasonable, performance for detecting suspected acute infarct. The overall findings suggest that the developed algorithms could be serially used in combination as a potential noncontrast-enhanced head CT critical finding screening tool for radiologists.

It is unclear whether section thickness contributed to the underdetection of some of the urgent findings, and further evaluation of the algorithm with thin-section images would be needed to assess for improved sensitivity. Nevertheless, while the clinical impact of missing subdural hematomas is not clearly known, previous reports suggest that a large proportion of small extra-axial hematomas may not require intervention (8).

Other studies have also investigated the performance of computer algorithms in detecting critical findings at noncontrast-enhanced head CT. Yuh et al (9) developed a customized algorithm to detect critical findings at noncontrast-enhanced head CT with sensitivity not statistically different to our method at 98% (95% CI: 88%, 100%), but with statistically lower specificity at 59% (95% CI: 51%, 67%) for acute intracranial hemorrhage and 57% (95% CI: 48%, 65%) for all critical findings. In addition, Li et al (10) created an algorithm to detect subarachnoid hemorrhage at noncontrast-enhanced head CT with reported performance of 100% sensitivity and 92.4% specificity. Last, Xiao et al (11) reported sensitivity of 94% and specificity of 100% to detect midline shift higher than 5 mm. However, these algorithms do not offer a solution for simultaneously detecting a range of urgent findings as described in our study.

Figure 5

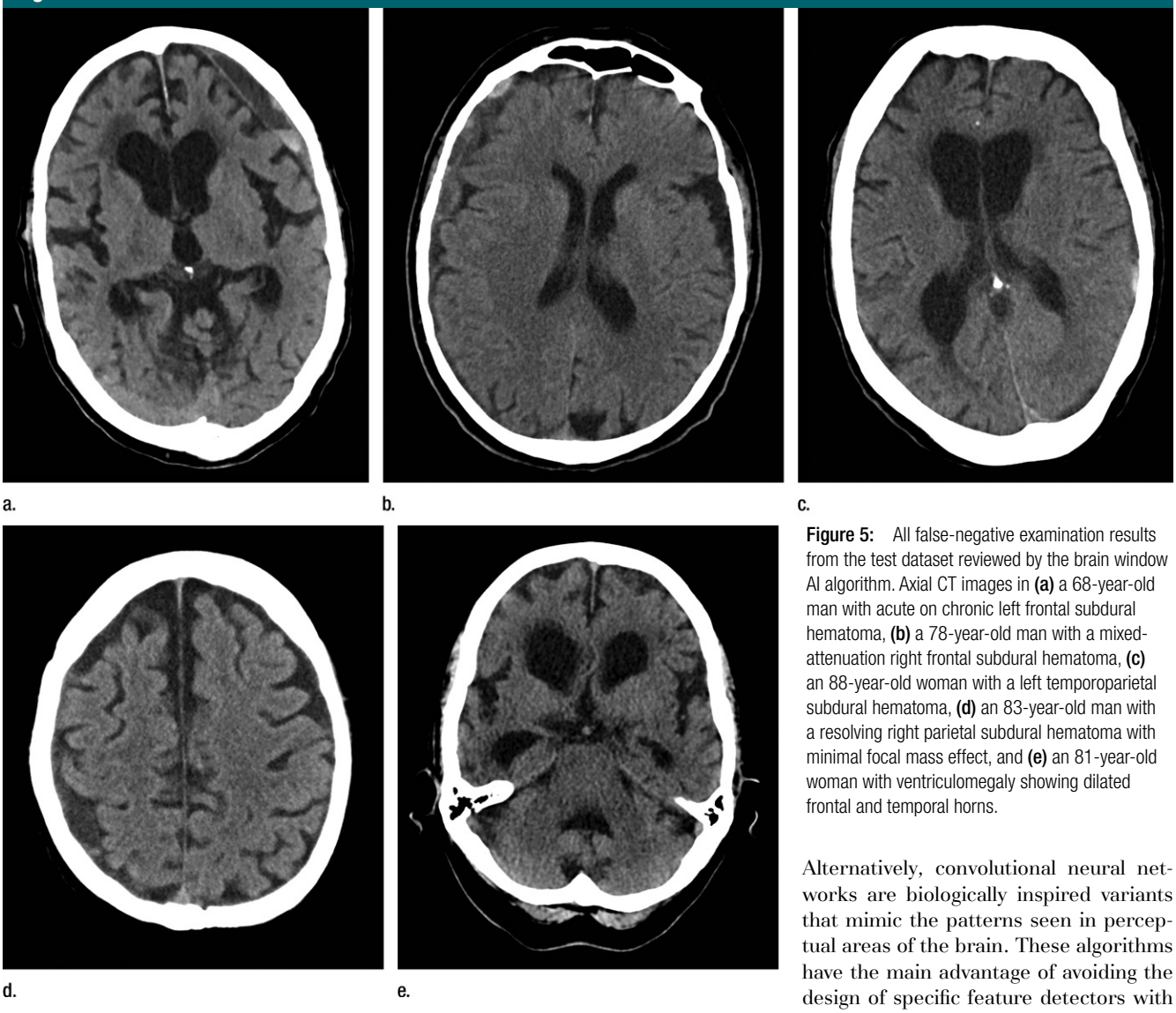

Figure 5: All false-negative examination results from the test dataset reviewed by the brain window AI algorithm. Axial CT images in **(a)** a 68-year-old man with acute on chronic left frontal subdural hematoma, **(b)** a 78-year-old man with a mixed-attenuation right frontal subdural hematoma, **(c)** an 88-year-old woman with a left temporoparietal subdural hematoma, **(d)** an 83-year-old man with a resolving right parietal subdural hematoma with minimal focal mass effect, and **(e)** an 81-year-old woman with ventriculomegaly showing dilated frontal and temporal horns.

Recognition of acute infarct at noncontrast-enhanced head CT is an important but secondary finding in the emergent setting because by the time hypoattenuation is detected, the area has likely already undergone irreversible ischemic damage (12). In addition, noncontrast-enhanced head CT is insensitive to show early signs of acute ischemia in the limited time span conducive to thrombolytic therapy (13). Prior reports show that radiologists have a range from 48% to 69% sensitivity and 84% to 100% specificity to detect early ischemic changes at noncontrast-enhanced head CT (14,15). Nagel et al (16) found no statistical difference between their algorithm and neuroradiologists in scoring acute ischemic changes at noncontrast-enhanced head CT, with sensitivities of 44% versus 44% and specificities of 93% versus 91%, respectively. Our stroke algorithm yielded similar performance in detecting early ischemic signs.

One of the major differences between our approach and previous work relates to the algorithm used, with the majority of prior reports using customized algorithms tailored to address only one specific clinical scenario (9,10). Alternatively, convolutional neural networks are biologically inspired variants that mimic the patterns seen in perceptual areas of the brain. These algorithms have the main advantage of avoiding the design of specific feature detectors with remarkable results, particularly in computer vision classification tasks (17–20). In addition, this approach is extremely fast to process on dedicated hardware.

A shortcoming of convolutional neural networks is the associated inability to precisely identify how the AI algorithm derived its conclusion, and the algorithm has the potential to function as a black box (21,22). Fine tuning the model may not be as straightforward as with narrowly focused algorithms. The system learns from images and labels provided during the training experience. If a consistent error is made, exposing the algorithm to more subtle or a higher

Figure 6

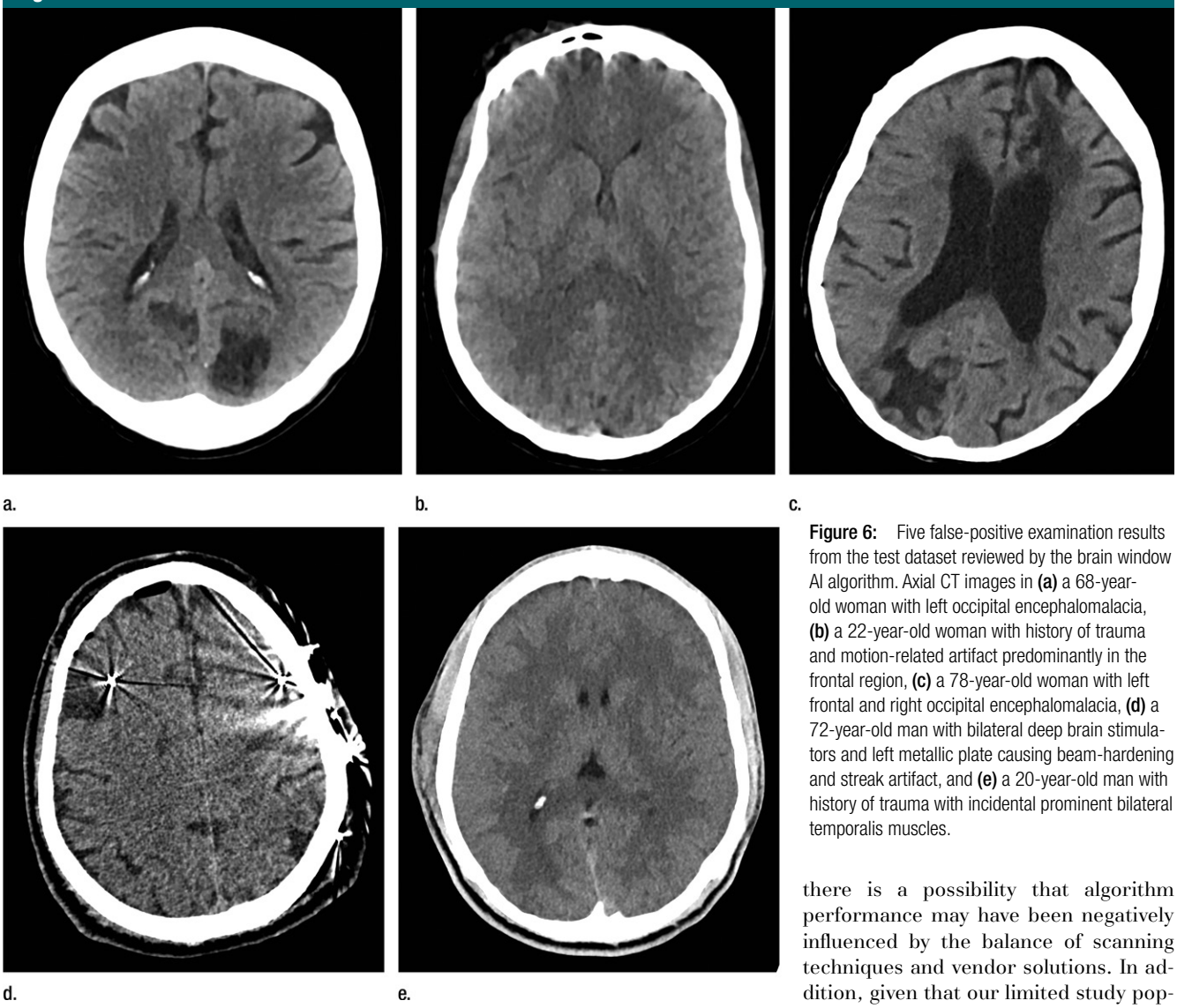

Figure 6: Five false-positive examination results from the test dataset reviewed by the brain window AI algorithm. Axial CT images in **(a)** a 68-year-old woman with left occipital encephalomalacia, **(b)** a 22-year-old woman with history of trauma and motion-related artifact predominantly in the frontal region, **(c)** a 78-year-old woman with left frontal and right occipital encephalomalacia, **(d)** a 72-year-old man with bilateral deep brain stimulators and left metallic plate causing beam-hardening and streak artifact, and **(e)** a 20-year-old man with history of trauma with incidental prominent bilateral temporalis muscles.

number of examinations may be a way to address errors, but algorithms may also have inherent limits; further research is needed in this realm. If additional pathologic findings are introduced at a later time, the algorithm would need to be retrained with the entire original dataset. Alternatively, serial algorithms, such as described in this report, could be built. There are also mechanisms to feed responses back into the algorithm so that it can be readjusted over time. However, this would have to be thoroughly tested as these readjustments could affect algorithm performance for other clinical scenarios.

Our findings support the need for further investigation of the two algorithms prospectively in a controlled clinical setting to determine whether they can independently screen noncontrast-enhanced head CT examinations. If successfully implemented, such a tool would help institutions meet national standards for communication of critical results (23).

This preliminary study had several limitations. Although we have included a variety of CT scanners in our dataset, there is a possibility that algorithm performance may have been negatively influenced by the balance of scanning techniques and vendor solutions. In addition, given that our limited study population was composed of consecutively acquired noncontrast-enhanced head CT examinations, we were not in control of the types of diseases selected; it is possible that the resulting case mix does not comprehensively encompass all important critical findings at noncontrast-enhanced head CT examinations. Last, our current algorithms do not take into consideration prior imaging studies and evolution of the disease. Nevertheless, we believe that our methodology offers a practical solution to the need for earlier recognition of critical findings in busy radiology practices without the resources to immediately

review noncontrast-enhanced head CT examinations on their completion.

While it is too early to know what will be the exact future role of AI and deep learning in radiology, current performance in the medical imaging domain has shown promising results. The use of AI for proactive screening and detection of urgent imaging findings may prove to be a practical and acceptable workflow enhancement for radiologists. On the basis of our preliminary experience, we foresee potential for rapid adoption and further expansion of AI methodology to support treatment decisions and improve radiology operationally in the future.

Disclosures of Conflicts of Interest: L.M.P. Activities related to the present article: received philanthropy from Edward J. DeBartolo, Jr Family. Activities not related to the present article: disclosed no relevant relationships. Other relationships: disclosed no relevant relationships. **B.S.E.** disclosed no relevant relationships. **J.L.R.** Activities related to the present article: received philanthropy from Edward J. DeBartolo, Jr Family. Activities not related to the present article: disclosed no relevant relationships. Other relationships: disclosed no relevant relationships. **K.J.L.** Activities related to the present article: received philanthropy from Edward J. DeBartolo, Jr Family. Activities not related to the present article: disclosed no relevant relationships. Other relationships: disclosed no relevant relationships. **M.D.** Activities related to the present article: received philanthropy from Edward J. DeBartolo, Jr Family. Activities not related to the present article: disclosed no relevant relationships. Other relationships: disclosed no relevant relationships. **S.Q.** Activities related to the present article: received philanthropy from Edward J. DeBartolo, Jr Family. Activities not related to the present article: disclosed no relevant relationships. Other relationships: disclosed no relevant relationships. **R.D.W.** Activities related to the present article: received philanthropy from Edward J. DeBartolo, Jr Family. Activities not related to the present article: disclosed no relevant relationships. Other relationships: disclosed no relevant relationships.

References

1. Chan KT, Carroll T, Linnau KF, Lehnert B. Expectations among academic clinicians of inpatient imaging turnaround time: does it correlate with satisfaction? Acad Radiol 2015;22(11):1449–1456.
2. Ioffe S, Szegedy C. Batch normalization: accelerating deep network training by reducing internal covariate shift. arXiv Prepr arXiv 150203167. https://arxiv.org/abs/1502.03167. Published 2015. Accessed June 14, 2017.
3. Wu R, Yan S, Shan Y, Dang Q, Sun G. Deep image: scaling up image recognition. arXiv Prepr arXiv 150102876. https://arxiv.org/abs/1501.02876. Published 2013. Accessed June 14, 2017.
4. Szegedy C, Vanhoucke V, Ioffe S, Shlens J, Wojna Z. Rethinking the inception architecture for computer vision. Proc IEEE Comput Soc Conf Comput Vis Pattern Recognit 2015;2015:2818–2826.
5. Chockley K, Emanuel E. The end of radiology? three threats to the future practice of radiology. J Am Coll Radiol 2016;13(12 Pt A):1415–1420.
6. Greenspan H, van Ginneken B, Summers MR. Guest editorial: deep learning in medical imaging—overview and future promise of an exciting new technique. IEEE Trans Med Imaging 2016;35(5):1153–1159.
7. Sarmanova A, Albayrak S. Alleviating class imbalance problem in data mining. Signal Processing and Communications Applications Conference, 2013 21st. IEEE; 2013; 1–4.
8. Bajsarowicz P, Prakash I, Lamoureux J, et al. Nonsurgical acute traumatic subdural hematoma: what is the risk? J Neurosurg 2015;123(5):1176–1183.
9. Yuh EL, Gean AD, Manley GT, Callen AL, Wintermark M. Computer-aided assessment of head computed tomography (CT) studies in patients with suspected traumatic brain injury. J Neurotrauma 2008;25(10):1163–1172.
10. Li YH, Zhang L, Hu QM, Li HW, Jia FC, Wu JH. Automatic subarachnoid space segmentation and hemorrhage detection in clinical head CT scans. Int J CARS 2012;7(4):507–516.
11. Xiao F, Liao CC, Huang KC, Chiang IJ, Wong JM. Automated assessment of midline shift in head injury patients. Clin Neurol Neurosurg 2010;112(9):785–790.
12. von Kummer R, Bourquain H, Bastianello S, et al. Early prediction of irreversible brain damage after ischemic stroke at CT. Radiology 2001;219(9):95–100.
13. de Lucas EM, Sánchez E, Gutiérrez A, et al. CT protocol for acute stroke: tips and tricks for general radiologists. RadioGraphics 2008;28(6):1673–1687.
14. Camargo EC, Furie KL, Singhal AB, et al. Acute brain infarct: detection and delineation with CT angiographic source images versus nonenhanced CT scans. Radiology 2007;244(2):541–548.
15. Takahashi N, Lee Y, Tsai DY, et al. Improvement of detection of hypoattenuation in acute ischemic stroke in unenhanced computed tomography using an adaptive smoothing filter. Acta Radiol 2008;49(7):816–826.
16. Nagel S, Sinha D, Day D, et al. e-ASPECTS software is non-inferior to neuroradiologists in applying the ASPECT score to computed tomography scans of acute ischemic stroke patients.. Int J Stroke doi:10.1177/1747493016681020. Published online December 1, 2016.
17. Li R, Zhang W, Suk HI, et al. Deep learning based imaging data completion for improved brain disease diagnosis. Med Image Comput Comput Assist Interv 2012;17(Pt 3):305–312.
18. Ramakrishnan K, Scholte S, Lamme V, et al. Convolutional neural networks in the brain: an fMRI study. J Vis 2015;15(12):371.
19. Chen X, Xu Y, Wong DW, Wong TY, Liu J. Glaucoma detection based on deep convolutional neural network. Conf Proc IEEE Eng Med Biol Soc 2015;2015:715–718.
20. Ypsilantis PP, Siddique M, Sohn HM, et al. Predicting response to neoadjuvant chemotherapy with PET imaging using convolutional neural networks. PLoS One 2015;10(9):e0137036.
21. Maier O, Schröder C, Forkert ND, Martinetz T, Handels H. Classifiers for ischemic stroke lesion segmentation: a comparison study. PLoS One 2015;10(12):e0145118. [Published correction appears in PLoS One 2016;11(2):e0149828.]
22. McLaren CE, Chen WP, Nie K, Su MY. Prediction of malignant breast lesions from MRI features: a comparison of artificial neural network and logistic regression techniques. Acad Radiol 2009;16(7):842–851.
23. National Patient Safety Goals. http://www.jointcommission.org/assets/1/6/2015_NPSG_HAP.pdf. Published 2015. Accessed February 4, 2017.